RSC Advances

PAPER

View Article Online
View Journal | View Issue

Cite this: *RSC Adv.*, 2022, **12**, 32979

Study on the long time aging behavior of $MAPbI_3$: from experiment to first-principles simulation†

Yan Li, ‡*[ae] Yu-Jing Dong,‡[bc] Hong He,[a] Xue-Lian Chen,[a] Hao Jiang [a] and Yu Jia *[bd]

As the core functional layer of perovskite solar cells, the serious issues of the $CH_3NH_3PbI_3$ film related to the long-term stability and its rapid degradation when exposed to the environment should be investigated deeply. In this study, the variation of phase construction, light absorption ability and fluorescence quenching ability during the long time aging process have been monitored. The results show that the degradation process is composed of the original serious fluorescence quenching and the lag behind phase decomposition. Then, the intrinsic physical mechanism has been obtained by the first-principles simulation of defect properties, which shows that the original serious fluorescence emission quenching is attributed to the deep level defects with low formation energies (such as V_{Pb} and I_{Pb}); meanwhile, the lag behind phase decomposition is caused by the easy ionic diffusion; for example, the diffusion activation energy of the iodine ion is 0.286 eV. The results illustrate that both the defect passivation and prevention of the ion diffusion are necessary for achieving a stable perovskite film.

Received 27th August 2022
Accepted 2nd November 2022

DOI: 10.1039/d2ra05378k

rsc.li/rsc-advances

1. Introduction

$CH_3NH_3PbI_3$ ($MAPbI_3$) based perovskite solar cells are one of the earliest and classical perovskite solar cell (PSC) types. The $MAPbI_3$ material is responsible for harvesting light, converting light into excitons and transporting excitons under sunlight. It shows the ability of broadband light absorption range, low exciton binding energy, long carrier diffusion length and high charge carrier mobility,[1–3] which boost the conversion efficiency of PSCs to almost 20% in the first few years. Nowadays, to prolong the lifetime of the PSCs, the systematic investigation of the phase decomposition, defect properties and ionic diffusion of the $MAPbI_3$ materials becomes increasingly significant.

In the beginning, the researchers found that the $MAPbI_3$ material is composed of an inorganic Pb–I octahedron and organic $CH_3NH_3^+$, and the organic and inorganic parts are brought together by van der Waals force, which leads to the easy breakdown of the perovskite structure under an external environment.[4–6] Common conclusions have shown that moisture, oxygen and light soaking are all the main reasons for the degradation of the perovskite materials. It is confirmed that the failure processes of $MAPbI_3$ under moisture should be the $CH_3NH_3^+$ being deprotonated by water, and then forming methylamine, hydrated HI and PbI_2.[7] The failure process of $MAPbI_3$ being exposed to oxygen and light soaking is because of the reaction of superoxide (O_2^-) between the photo-generated electrons and O_2, yielding methylamine, PbI_2 and I_2 as products.[8,9] At this research stage, in order to detect the reaction products accurately, the failure behavior can be traced by some kinds of a precision testing equipment; for example, Yang *et al.*[10] used *in situ* absorption spectroscopy and *in situ* grazing incidence X-ray diffraction to monitor chemical changes, and found that the formation of a hydrated intermediate containing isolated PbI_6^{4-} octahedra was the first step of the degradation processes. Shi *et al.*[11] used gas chromatography-mass spectrometry to verify the gas compositions during the degradation of the multi-cation perovskite precursors, and they identified the decomposition products as CH_3I, NH_3, and so on.

As the research investigation moved forward, researchers found that before the van der Waals bond was broken down under the environment, defect properties and ion diffusion must be considered. Considering original defect properties and ionic diffusion are hard to detect by equipment, first principles study has usually been proposed to uncover the changes in crystal structures. The first principles studies show 12 intrinsic point defects in the $MAPbI_3$ materials, including vacancies (V_{MA}, V_{Pb}, and V_I), interstitials (MA_I, Pb_I, and I_I) and antisites

[a]School of Materials Science and Engineering, Xi'an Shiyou University, Xi'an, 710065, China. E-mail: yli@xsyu.edu.cn

[b]Key Laboratory for Special Functional Materials of Ministry of Education, School of Materials, Center for Topological Functional Materials, School of Physics and Electronic, Henan University, Kaifeng 475001, China. E-mail: jiayu@henu.edu.cn

[c]School of Science and Technology, Xinyang College, Xinyang 464000, China

[d]International Laboratory for Quantum Functional Materials of Henan, School of Physics, Zhengzhou University, Zhengzhou 450001, China

[e]State Key Laboratory for Mechanical Behavior of Materials, Xi'an Jiaotong University, Xi'an, 710065, China

† Electronic supplementary information (ESI) available. See DOI: https://doi.org/10.1039/d2ra05378k

‡ The first two authors contribute equally to this research.

(MA_{Pb}, Pb_{MA}, MA_I, Pb_I, I_{MA}, and I_{Pb}).[12] The calculation results also show that most vacancies produce shallow trap states near the band edge, but deep level defects (such as interstitial and antisite defects) may exist at the surface and grain boundaries of the perovskite films. In detail, it is considered that the defect densities on the surface are five orders of magnitude larger than that in the interior.[13,14] The defects will cause nonradiative recombination and affect the ionic diffusion.[15,16] As to the correlation between the phase decomposition, defect property and ion diffusion, Yuan *et al.*[17] applied simultaneous luminescence and electron microscopy on the perovskite to monitor *in situ* morphology evolution and optical properties, and they pointed out that during the degradation process, the defects were created in the perovskite first, and then, the directional ion diffusion would be driven by these defects, which altered the fluorescence intensity and changed the chemical composition finally. Zhang *et al.*[18] studied the role of iodine in the degradation of $MAPbI_3$ by *ab initio* simulation, and they thought that excess electrons or holes would enhance I^- radical adsorption and its reaction with $MAPbI_3$ surfaces. Wang *et al.*[19] emphasized that the diffusion and accumulation of charged ions directly lead to significant changes in the doping concentration of the perovskite film and the built-in electric field, which were the key factors affecting the stability of PSCs. It can be seen that the defect property and ion diffusion play an important role in the degradation process of the $MAPbI_3$ films.

In this study, $MAPbI_3$ films of uniform quality have been prepared, and the long time aging behaviors, including the variation of phase construction, light absorption ability and fluorescence quenching ability of the perovskite films, under series conditions have been monitored by fluorescence emission spectrometry, UV-visible absorption spectrometry and X-ray diffraction spectrometry. Subsequently, the trap properties and the ion diffusion have been used to explain the initial serious fluorescence quenching and the lag behind phase decomposition. Lastly, the degradation process of the $MAPbI_3$ film has been explained by the formation of deep level trap states and the ion diffusion.

2. Experiment

2.1 Chemicals

Lead iodide (PbI_2) and methylammonium (CH_3NH_3I, MAI) purchased from *p*-OLED Co. (China) were used as solutes. *N*,*N*-Dimethylformamide (DMF) purchased from Adamas-beta (China) was used as the solvent. All the chemicals were of reagent grade and used without further purification. Transparent fluorine-doped tin oxide (FTO, TEC-15, LOF) conductive glasses (20 mm × 20 mm) were employed as substrates. Before the film deposition, the substrates were cleaned successively in deionized water and alcohol, and dried with N_2 flow.

2.2 Preparation of the $MAPbI_3$ film

For $MAPbI_3$ film preparation, first, PbI_2 and MAI are dissolved in the DMF solvent with a concentration of 460 mg ml^{-1}, and then kept at 70 °C for 30 min by using a laboratory type magnetic stirrer. Second, the prepared $MAPbI_3$ precursor solution was dropped on the surface of the FTO substrate, and subsequently, the substrate was spin-coated at 3000 rpm for 10 s and then was dried under a gas pumping pressure of 3000 Pa, which was controlled automatically by the equipment control unit.[20–22] Finally, the $MAPbI_3$ film was prepared. All the processes were carried out in air without inert gas protection, and the laboratory temperature was kept below 20 °C during the film preparation.

2.3 Long time aging test of the $MAPbI_3$ film

The full spectrum light source was provided by a solar simulator (Newport, Class AAA) with a 100 mW cm^{-2} xenon lamp (Sol3A, Oriel), and the UV source was proved by a monochromatic UV lamp with a wavelength of 365 nm and intensity of 20 mW cm^{-2} (S-939, Saibao). The aging test proceeded under full spectrum light and under an atmosphere, indicating with sunlight with air, coded as A_{ir}-AM 1.5. The aging test proceeded under full spectrum light in a N_2 glove box, indicating with sunlight without air, coded as N_2-AM 1.5. The aging test proceeded under UV irradiation and under an atmosphere, indicating with UV with air, coded as A_{ir}-UV.

During the long time aging process, the phase construction of the perovskite films was measured using an X-ray diffractometer with Cu K_α radiation (XRD, Bruker, Germany). The absorption ability of the perovskite films was quantitatively analyzed using a UV-visible spectrophotometer (UV-vis., Shimadzu U-2700, Japan). The fluorescence quenching ability is measured using a high sensitivity spectrometer (PL, Maya2000Pro, Ocean Optics, China) at an excitation wavelength of 560 nm. The morphology of the $MAPbI_3$ film was characterized using a scanning electron microscope (TSCAN, The Czech Republic).

2.4 Calculation methods and models

All the calculations are accomplished by density functional theory (DFT) using the generalized gradient approximation (GGA) within the Perdew–Burke–Ernzerhof (PBE)[23] level and the plane-wave pseudopotential approach as implemented in the Vienna *ab initio* simulation package (VASP).[24] A kinetic energy cutoff of 400 eV is used for the plane-wave basis set and geometries are relaxed until a residual force less than 0.02 eV per Å per atom. The supercell containing 2 × 2 unit cells is employed to make sure enough distance (>12 Å) and avoid the interaction between defects. It is important to determine the number of layers of the surface structure. Because the surface energy changes little with the atomic layer thickness larger than three layers, the thickness of four atomic layers was selected to calculate the surface defect properties, and the bottom fixed two layers were chosen as the bulk properties in the further calculation. The total energy of a charged system was not considered due to the electrostatic repulsion between slabs.[25] The DFT simulations also include van der Waals correction of Grimme and coworkers[26,27] to treat the weak interaction of organic–inorganic perovskites. The activation energy of iodine vacancy-

assisted ion diffusion was obtained by the climbing image nudged elastic band (CI-NEB) method.[28]

3. Results and discussion

3.1 Microstructures of the $MAPbI_3$ films

The architecture of the prepared $MAPbI_3$ sample is presented in Fig. 1a. It is composed of a rough FTO substrate and a ~400 nm $MAPbI_3$ film, and the detailed morphology information was discussed in the previous literature.[29] The appearance of the $MAPbI_3$ film by the naked eyes is shown in Fig. 1b and c, and all the samples show a uniform dark brown color and mirror like surface. The surface microstructure of the perovskite film is shown in Fig. 1d and e, as can be seen there is a uniform full coverage surface and condensed grains without pinholes in low magnification, and the grain size is less than 500 nm in high magnification.

Furthermore, the $MAPbI_3$ films are divided into three groups, which individually undergo a long time aging test for 6 h under an air atmosphere with AM1.5 illumination, under a N_2 atmosphere with AM1.5 illumination, and under an air atmosphere with UV 365 nm irradiation. The samples are coded as A_{ir}-AM1.5, N_2-AM1.5 and A_{ir}-UV correspondingly.

3.2 The long time aging behaviors of the $MAPbI_3$ film

The PL, UV-vis and XRD data have been characterized each hour. The original data are added in the ESI,† as shown in

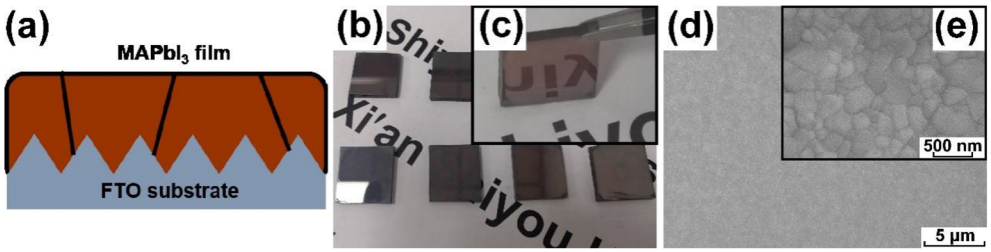

Fig. 1 The $MAPbI_3$ film deposited on the substrate: (a) schematic diagram, (b) and (c) photograph appearance, and (d) and (e) scanning electron microscope images under high and low resolutions.

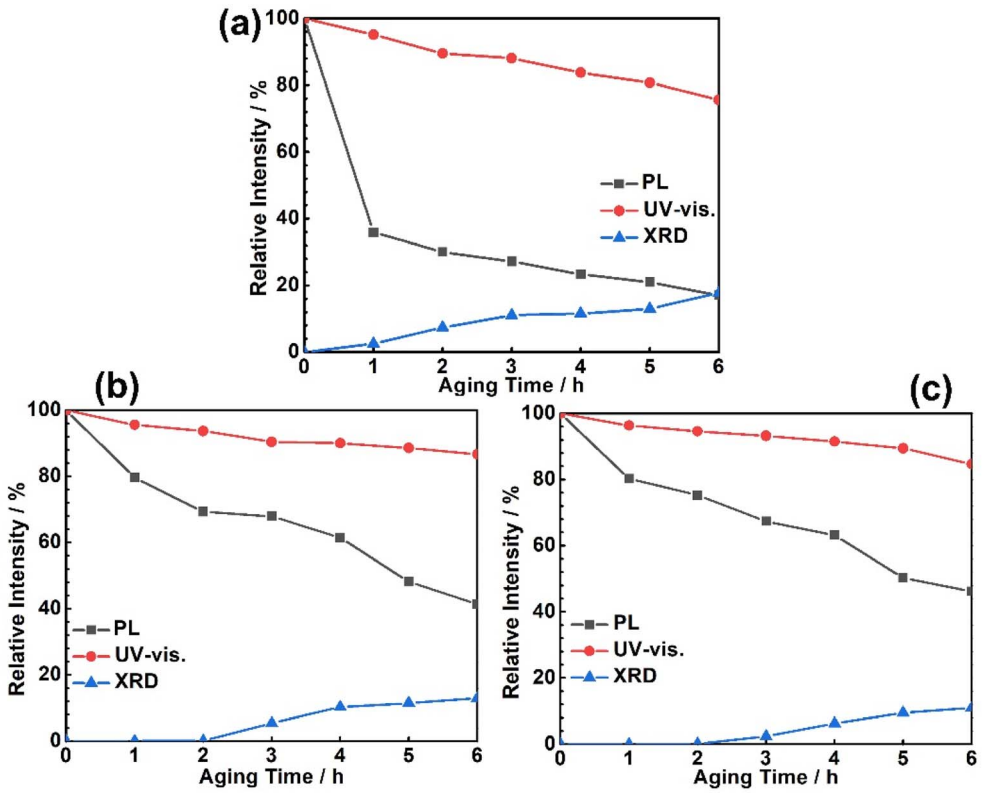

Fig. 2 The long time aging behaviors of the $MAPbI_3$ under the series conditions: (a) under an air atmosphere with AM1.5 illumination (A_{ir}-AM1.5), (b) under a N_2 atmosphere with AM1.5 illumination (N_2-AM1.5) and (c) under an air atmosphere with UV illumination (A_{ir}-UV). The original data are listed in Fig. S1 to S3.† To reach Fig. 2, the reference wavelength of the PL is chosen as 770 nm, and the reference wavelength of UV-vis is chosen as 500 nm, and also the reference 2θ degree of XRD is chosen as 12.7°. The PL, UV-vis and XRD data at 0 h are defined as 100%.

Fig. S1 (A_{ir}-AM1.5), S2 (N_2-AM1.5) and S3† (A_{ir}-UV), and the relative intensity trends of the three conditions are listed in Fig. 2. To summarize the results in Fig. 2, the reference wavelength of the PL is chosen as 770 nm, and the reference wavelength of UV-vis is chosen as 500 nm, and also, the reference 2θ degree of XRD is chosen as 12.7°. The PL, UV-vis and XRD data at 0 h are defined as 100%.

As can be seen in Fig. 2, the absorption ability and fluorescence quenching ability of the $MAPbI_3$ film under the three conditions, A_{ir}-AM1.5, N_2-AM1.5 and A_{ir}-UV, all decline obviously at the original aging time; however, the XRD results coming from the (001) plane of PbI_2 appear when the aging test reaches a certain time; for example, the PbI_2 appears at the aging time of 1 h, 3 h and 3 h for A_{ir}-AM1.5, N_2-AM1.5 and A_{ir}-UV based on Fig. S1(a), S2(a) and S3(a),† respectively. In addition, a faster failure rate under A_{ir}-AM1.5 compared with both of N_2-AM1.5 and A_{ir}-UV is found in this experiment.

Compared with the PL and XRD data, we found that the fluorescence quenching seems more sensitive to the aging process compared with phase decomposition. As can be seen in Fig. 2a, the fluorescence quenching ability decreased ~60%; however, the PbI_2 phase only increased ~5% when the aging time went on to 1 h under the A_{ir}-AM1.5 condition. The fluorescence quenching ability decreased to 80%, and only ~20% increase of PbI_2 was characterized when the aging time went on to 4 h. The relative intensities show the same tendency under N_2-AM1.5 and A_{ir}-UV conditions, indicating that there is a serious PL quenching at first, and the phase decomposition of the $MAPbI_3$ film lags behind the fluorescence quenching. Considering that both the defect properties and ion diffusion play an important role in the degradation process of the $MAPbI_3$ films, we use the first-principles simulation to establish the fundamental physics interpretation from the original fluorescence quenching and the subsequent phase decomposition in the following.

3.3 The initial serious PL quenching of the $MAPbI_3$ film

The defect states in the $MAPbI_3$ film have been simulated. The as-prepared $MAPbI_3$ crystal film is a tetragonal structure with the parameters of $a = b = 8.91$ Å and $c = 13.14$ Å, which is in agreement with the previous XRD results ($a = b = 8.97$ Å, $c = 13.16$ Å).[29] When it is cut parallel to the (110) panel, the possible surface forms of the $MAPbI_3$ crystal are listed in Fig. 3. The surface energies of the stoichiometric atom ratio and the nonstoichiometric atom ratio of $MAPbI_3$ surfaces are calculated based on eqn (1) and eqn (2), separately. All the calculated surface energies are shown in Table 1, which shows that the surface energy of MAI-termination with a nonstoichiometric atom ratio of $MAPbI_3$ (MAI-non) is the lowest compared to those of the other three surfaces, which is chosen and considered in the following investigation.

$$E_{\text{surface}} = \frac{1}{2A}\left(E_{\text{slad}} - nE_{\text{bulk}}\right) \quad (1)$$

$$E_{\text{surface}} = \frac{1}{2A}\left(E_{\text{slad}} - n_{\text{MAI}}\mu_{\text{MAI}} - n_{\text{PbI}_2}\mu_{\text{PbI}_2}\right) \quad (2)$$

where n refers to the number of atoms in the unit cell, and μ refers to the total energy of MAI or PbI_2.

In order to determine the easily formed defect types, we calculated the phase diagram of $MAPbI_3$, and the stable $MAPbI_3$ phase is shown in Fig. S4,† which will provide the chemical potential for the following defect formation energy calculation.

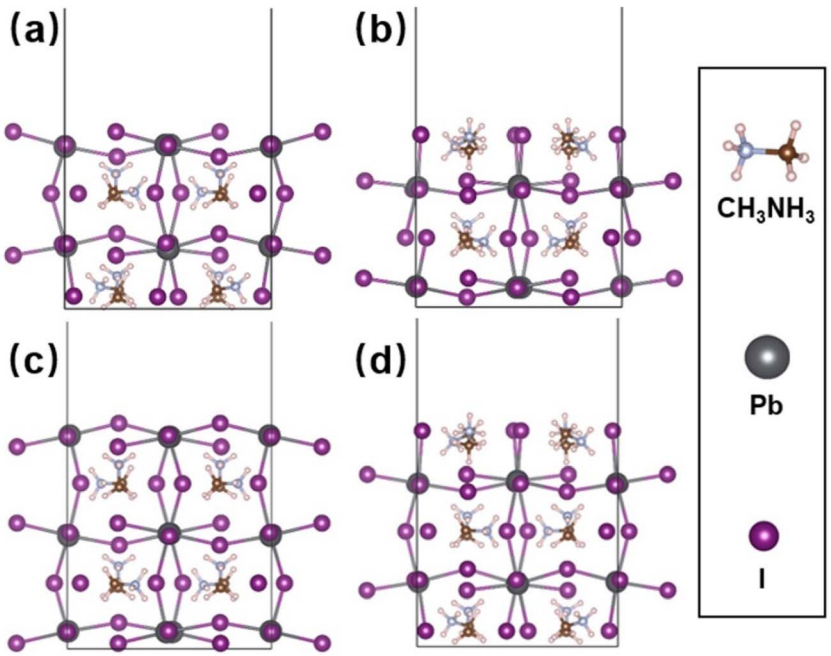

Fig. 3 The four possible surfaces of the $MAPbI_3$ crystal are stoichiometric atom ratio with MAI-termination (a) and with PbI_2-termination (b), and nonstoichiometric atom ratio with MAI-termination (c) and with PbI_2-termination (d).

Table 1 The surface energies of the four $MAPbI_3$ surfaces (meV $Å^{-2}$)

	PbI_2-termination	MAI-termination
Stoichiometric atom ratio	26.42	20.24
Nonstoichiometric atom ratio	31.38	17.72

Table 2 Considered types of surface defects and their formation energy (in eV) under different conditions; the types of surface defects include vacancies (V_{MA}, V_{Pb}, and V_I), interstitials (MA_i, Pb_i, and I_i) and anti-site substitutions (MA_I, I_{MA}, Pb_I, I_{Pb}, MA_{Pb}, Pb_{MA}, and A_B means A on B site)

MAI-non	I-poor	I-rich
V_{MA}	2.638	0.880
V_I	0.423	2.180
V_{Pb}	2.226	−1.289
MA_i	0.011	1.769
Pb_i	2.028	5.543
I_i	1.835	0.077
I_{MA}	3.700	0.185
MA_I	0.961	4.476
I_{Pb}	4.160	−1.112
Pb_I	2.106	7.379
MA_{Pb}	0.683	−1.075
Pb_{MA}	2.104	3.861

The defect types in the $MAPbI_3$ crystal and corresponding defect formation energies under both I-poor and I-rich chemical conditions are shown in Table 2. In general, the $MAPbI_3$ film prepared by the one-step solution method always produces a Pb-poor/I-rich component in the film,[30,31] and then, the corresponding defect energy level positions for the I-rich component are calculated and listed in Fig. 4. Based on Table 2 and Fig. 4, the defects of V_{Pb} and I_{Pb} not only show the lowest formation energy (negative data) but also are the deep level defect types, indicating their easy formation and easy to be non-radiation recombination centers.

In fact, in order to reach the uniform and full-coverage morphology, the rapid crystallization process is always chosen to prepare the perovskite film, for example the low pressure gap pumping method used in this research, and it usually results in a large amount of surface defects. At the same time, the external stimuli will also stimulate a large amount of defects under the long-time aging process. Based on these reasons, the large amount of defects, particularly the deep level defects V_{Pb} and I_{Pb} with low formation energies, will form non-radiation recombination centers and capture carriers, which may induce a serious fluorescence quenching at the early aging time.

3.4 The lag behind phase degradation of the $MAPbI_3$ film

Then, the lag behind phase decomposition of the $MAPbI_3$ has also been analyzed. Previous results have proved that the abundant surface defects, mainly shallow-level defect halide vacancies, will act as ion diffusion channels, which will enlarge open circuit voltage loss, and hinder device advancements.[32] In the working environment, the formation of shallow-level defects is promoted through the influence of light and electricity, resulting in enhanced ion diffusion. In addition, the chemical bond is easy to break down under light, heat and other conditions. Taking the Pb–I bond as an example, the diffusion energy of I^- in $MAPbI_3$ crystals has been calculated and is shown in Fig. 5. The energy barrier for I^- diffusion is 0.286 eV.

Previous results not only proved that the ionic diffusion can recover when the trigger was removed,[33] but also pointed that the more easy the diffusion of ions, for example I^-, the more easy the escape of $CH_3NH_3^+$ from being bound by the I–Pb octahedra,[34] which would induce the collapse of the octahedron structure in the long time aging process. Therefore, the phase decomposition lags behind the fluorescence quenching, can be illustrated that, more and more defects appear with proceeding the light irradiation, and the ion diffusion is not only enhanced, but also be irreversible, therefore both the continuous decrease of the fluorescence quenching and a lag behind phase decomposition are two important effect factors for the high performance and stability $MAPbI_3$ film.

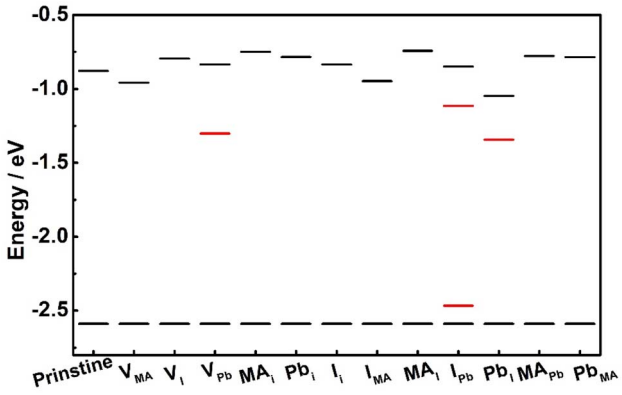

Fig. 4 The various defect types in $MAPbI_3$ crystals and the corresponding energy level positions.

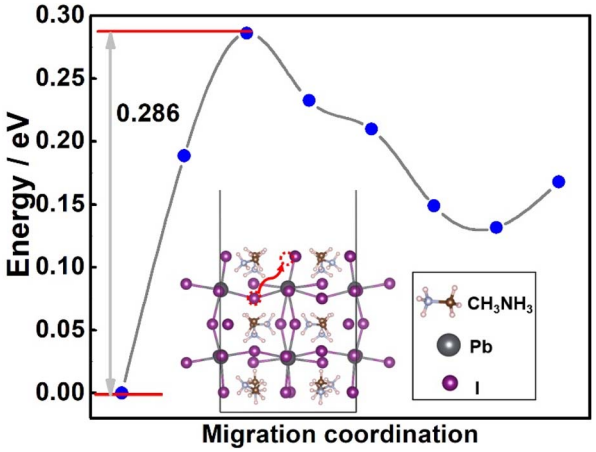

Fig. 5 The diffusion energy of I^- in the $MAPbI_3$ surface. The inset figure is the diffusion path of I^- when I vacancy defects exist.

4. Conclusion

In this study, fluorescence quenching and phase decomposition, both important for identifying the quality of the perovskite film, have been investigated through a long time aging analysis. Based on the experimental results, it can be noticed that there is a serious PL quenching in the first stage, followed by a lag behind phase degradation. Combined with the first-principles simulation to analyze the defect properties and ion diffusion, there are deep level defect types with low formation energies, including V_{Pb} and I_{Pb} in the $MAPbI_3$ film, and the diffusion energy barrier of the I^- in the $MAPbI_3$ film is 0.286 eV. Therefore, it can be concluded that the degradation process is composed of two periods, the original fluorescence quenching and the subsequent phase decomposition. At the early aging stage, the easily formed deep level defects are responsible for the decrease of the fluorescence quenching. With the proceeding of the aging time, the irreversible ion diffusion will lead to the phase decomposition. The degradation processes gained from this study are important for designing stable perovskite films, and it proves that both the defect passivation and preventing the ion diffusion are necessary for achieving a stable perovskite film.

Conflicts of interest

There are no conflicts to declare.

Acknowledgements

All the authors acknowledge financial support from State Key Laboratory for Mechanical Behavior of Materials and National Natural Science Foundation of China (Grant No. 62104191).

References

1 J. Xiao and H. L. Zhang, Recent progress in organic–inorganic hybrid perovskite materials for luminescence applications, *Acta Phys.-Chim. Sin.*, 2016, **32**, 1894–1912.
2 F. Li, C. Ma, H. Wang, W. Hu, W. Yu, A. D. Sheikh and T. Wu, Ambipolar solution-processed hybrid perovskite phototransistors, *Nat. Commun.*, 2015, **6**, 8238.
3 D. Shi, V. Adinolfi, R. Comin, M. J. Yuan, E. Alarousu, A. Buin, Y. Chen, S. Hoogland, A. Rothenberger, K. Katsiev, Y. Losovyj, X. Zhang, P. A. Dowben, O. F. Mohammed, E. H. Sargent and O. M. Bakr, Low trap-state density and long carrier diffusion in organolead trihalide perovskite single crystals, *Science*, 2015, **347**, 519–522.
4 N. Li, X. Niu, Q. Chen and H. Zhou, Towards commercialization: the operational stability of perovskite solar cells, *Chem. Soc. Rev.*, 2020, **49**, 8235–8286.
5 Q. Guo, J. X. Zhao, K. Zhou, B. Y. Xing, X. J. Wang, F. Y. Tian, X. He and L. Zhang, High-throughput computational material screening of the cycloalkane-based two-dimensional Dion-Jacobson halide perovskites for optoelectronics, *Chin. Phys. B*, 2022, **31**, 37104.
6 J. Xin, P. Z. Yang, J. P. Wang and S. H. Wei, Theoretical investigation of halide perovskites for solar cell and optoelectronic applications, *Chin. Phys. B*, 2020, **29**, 108401.
7 J. A. Christians, P. A. Miranda Herrera and P. V. Kamat, Transformation of the excited state and photovoltaic efficiency of $CH_3NH_3PbI_3$ perovskite upon controlled exposure to humidified air, *J. Am. Chem. Soc.*, 2015, **137**, 1530–1538.
8 N. Aristidou, I. Sanchez-Molina, T. Chotchuangchutchaval, M. Brown, L. Martinez, T. Rath and S. A. Haque, The role of oxygen in the degradation of methylammonium lead trihalide perovskite photoactive layers, *Angew. Chem., Int. Ed.*, 2015, **54**, 8208–8212.
9 G. Niu, W. Li, F. Meng, L. Wang, H. Dong and Y. Qiu, Study on the stability of $CH_3NH_3PbI_3$ films and the effect of post-modification by aluminum oxide in all-solid-state hybrid solar cells, *J. Mater. Chem. A*, 2014, **2**, 705–710.
10 J. L. Yang, B. D. Siempelkamp, D. Y. Liu and T. L. Kelly, Investigation of $CH_3NH_3PbI_3$ degradation rates and mechanisms in controlled humidity environments using *in situ* techniques, *ACS Nano*, 2015, **9**, 1955–1963.
11 L. Shi, M. P. Bucknall, T. L. Young, M. Zhang, L. Hu, J. M. Bing, D. S. Lee, J. Kim, T. Wu, N. Takamure, D. R. McKenzie, S. J. Huang, M. A. Green and A. W. Y. Ho-Baillie, Gas chromatography-mass spectrometry analyses of encapsulated stable perovskite solar cells, *Science*, 2020, **368**, 1328.
12 Y. Yin, L. Li and W. J. Yin, Theoretical and computational study on defects of solar cell materials, *Acta Phys. Sin.*, 2020, **69**, 177101.
13 A. Hassan, Z. J. Wang, H. A. Yeong, M. Azam, A. A. Khan, U. Farooq, M. Zubair and Y. Cao, Recent defect passivation drifts and role of additive engineering in perovskite photovoltaics, *Nano Energy*, 2022, **101**, 107579.
14 Z. Y. Ni, C. X. Bao, Y. Liu, Q. Jiang, W. Q. Wu, S. S. Chen, X. Z. Dai, B. Chen, B. Hartweg, Z. S. Yu, Z. Holman and J. S. Huang, Resolving spatial and energetic distributions of trap states in metal halide perovskite solar cells, *Science*, 2020, **367**, 1352–1358.
15 J. M. Ball and A. Petrozza, Defects in perovskite-halides and their effects in solar cells, *Nat. Energy*, 2016, **1**, 1–13.
16 D. Luo, R. Su, W. Zhang, Q. Gong and R. J. Zhu, Minimizing non-radiative recombination losses in perovskite solar cells, *Nat. Rev. Mater.*, 2020, **5**, 44–60.
17 H. Yuan, E. Debroye, K. Janssen, H. Naiki and M. B. J. Roeffaers, Degradation of methylammonium lead iodide perovskite structures through light and electron beam driven ion diffusion, *J. Phys. Chem. Lett.*, 2016, **7**, 566.
18 L. Zhang and H. L. Sit, Ab initio study of the role of iodine in the degradation of $CH_3NH_3PbI_3$, *J. Mater. Chem. A*, 2017, **5**, 23976.
19 J. F. Wang, D. X. Lin and Y. B. Yuan, Recent progress of ion migration in organometal halide perovskite, *Acta Phys. Sin.*, 2019, **68**, 21.
20 B. Ding, L. Gao, L. Liang, Q. Chu, X. Song, Y. Li, G. Yang, B. Fan, M. Wang and C. Li, Facile and scalable fabrication of highly efficient lead iodide perovskite thin-film solar

cells in air using gas pump method, *ACS Appl. Mater. Interfaces*, 2016, **8**, 20067.

21 Y. Li, X. L. He, B. Ding, L. L. Gao, G. J. Yang, C. X. Li and C. J. Li, Realizing full coverage of perovskite film on substrate surface during solution processing: Characterization and elimination of uncovered surface, *J. Power Sources*, 2016, **320**, 204–211.

22 G. J. Yang, B. Ding, Y. Li, S. Y. Huang, Q. Q. Chu, C. Li and C. Li, Material nucleation/growth competition tuning towards highly reproducible planar perovskite solar cells with efficiency exceeding 20%, *J. Mater. Chem. A*, 2017, **5**, 6840–6848.

23 J. P. Perdew, K. Burke and M. Ernzerh, Generalized gradient approximation made simple, *Phys. Rev. Lett.*, 1996, **77**, 3865.

24 G. Kresse and D. Joubert, From ultrasoft pseudopotentials to the projector augmented-wave method, *Phys. Rev. B: Condens. Matter Mater. Phys.*, 1999, **59**, 1758–1775.

25 H. Uratani and K. Yamashita, Charge carrier trapping at surface defects of perovskite solar cell absorbers: a first-principles study, *J. Phys. Chem. Lett.*, 2017, **8**, 742–746.

26 S. Grimme, *J. Comput. Chem.*, 2006, **27**, 1787–1799.

27 V. Barone, M. Casarin, D. Forrer, M. Pavone, M. Sambi and A. Vittadini, Role and effective treatment of dispersive forces in materials: polyethylene and graphite crystals as test cases, *J. Comput. Chem.*, 2009, **30**, 934–939.

28 G. Henkelman and H. Jonsson, Improved tangent estimate in the nudged elastic band method for finding minimum energy paths and saddle points, *J. Chem. Phys.*, 2000, **113**, 9978–9985.

29 Y. Li, R. L. Z. Hoye, H. H. Gao, L. H. Yan, X. Y. Zhang, Y. Zhou, J. L. MacManus-Driscoll and J. Gan, Over 20% efficiency in methylammonium lead iodide perovskite solar cells with enhanced stability *via* "*in situ* solidification" of the TiO_2 compact layer, *ACS Appl. Mater. Interfaces*, 2020, **12**, 7135–7143.

30 X. C. Qiu, Y. Liu, W. W. Li and Y. Y. Hu, Traps in metal halide perovskites: characterization and passivation, *Nanoscale*, 2020, **12**, 22425–22451.

31 Y. Huang, W. J. Yin and Y. He, Intrinsic point defects in inorganic cesium lead iodide perovskite $CsPbI_3$, *J. Phys. Chem. C*, 2018, **122**, 1345–1350.

32 R. Partha, P. Sil, D. Sayantan, S. Arka and D. Dirtha, Investigation of ion-mediated charge transport in methylammonium lead iodide perovskite, *J. Phys. Chem. C*, 2017, **121**, 5515–5522.

33 W. Nie, J. C. Blancon, A. J. Neukirch, K. Appavoo, H. Tsai, M. Chhowalla, M. A. Alam, M. Y. Sfeir, C. Katan, J. Even, S. Tretiak, J. J. Crochet, G. Gupta and A. D. Mohite, Light-activated photocurrent degradation and self-healing in perovskite solar cells, *Nat. Commun.*, 2016, **7**, 11574.

34 T. A. Berhe, W. N. Su, C. H. Chen, C. J. Pan, J. H. Cheng, H. M. Chen, M. C. Tsai, L. Y. Chen, A. A. Dubale and B. J. Hwang, Organometal halide perovskite solar cells: degradation and stability, *Energy Environ. Sci.*, 2016, **9**, 323–356.